

# Intrinsic Dimension Estimating Autoencoder (IDEA) Using CancelOut Layer and a Projected Loss

Application to Vertically Resolved Shallow Flow Simulations

Antoine Oriou<sup>a,b,\*</sup>, Philipp Krah<sup>c</sup>, Julian Koellermeier<sup>a,d</sup>

<sup>a</sup>*Department of Mathematics, Computer Science and Statistics, University of Ghent*

<sup>b</sup>*CentraleSupélec, University Paris-Saclay*

<sup>c</sup>*IRFM, CEA Cadarache*

<sup>d</sup>*Bernoulli Institute, University of Groningen*

## Abstract

This paper introduces the Intrinsic Dimension Estimating Autoencoder (IDEA), which identifies the underlying intrinsic dimension of a wide range of datasets whose samples lie on either linear or nonlinear manifolds. Beyond estimating the intrinsic dimension, IDEA is also able to reconstruct the original dataset after projecting it onto the corresponding latent space, which is structured using re-weighted double CancelOut layers. Our key contribution is the introduction of the *projected reconstruction loss* term, guiding the training of the model by continuously assessing the reconstruction quality under the removal of an additional latent dimension.

We first assess the performance of IDEA on a series of theoretical benchmarks to validate its robustness. These experiments allow us to test its reconstruction ability and compare its performance with state-of-the-art intrinsic dimension estimators. The benchmarks show good accuracy and high versatility of our approach.

Subsequently, we apply our model to data generated from the numerical solution of a vertically resolved one-dimensional free-surface flow, following a pointwise discretization of the vertical velocity profile in the horizontal direction, vertical direction, and time. IDEA succeeds in estimating the dataset's intrinsic dimension and then reconstructs the original solution by working directly within the projection space identified by the network.

*Keywords:* autoencoder, intrinsic dimension, CancelOut layer, free-surface flow.

## 1. Introduction

The intrinsic dimension (ID)  $d$  of a dataset is a fundamental quantity that refers to the minimum number of parameters required to represent the data with satisfactory accuracy (Bac et al. (2021)). We consider datasets represented as matrices  $M \in \mathcal{M}_{n,p}(\mathbb{R})$  where, following standard machine learning notation,  $n$  denotes the number of samples and  $p$  the number of features. Such a dataset corresponds to a collection of points in  $\mathbb{R}^p$ , where  $p$  is the embedded dimension.

The objective is to determine the intrinsic dimension  $d < p$  of such datasets and to accurately reconstruct the data using only  $d$  parameters.

We illustrate this distinction with two contrasting examples where the intrinsic and embedded dimensions differ, shown in Figure 1.

In Figure 1a, the dataset consists of  $n$  sample points  $(x_i, y_i, z_i)$  such that  $x_i^2 + y_i^2 + z_i^2 = 1 \forall i \in \{1, \dots, n\}$ , describing points on a 2D sphere embedded in 3D space. Despite being represented in three dimensions, the data lies on a 2D surface. A well-designed model should infer that two parameters, such as azimuthal and polar angles, are sufficient to reconstruct the data without loss.

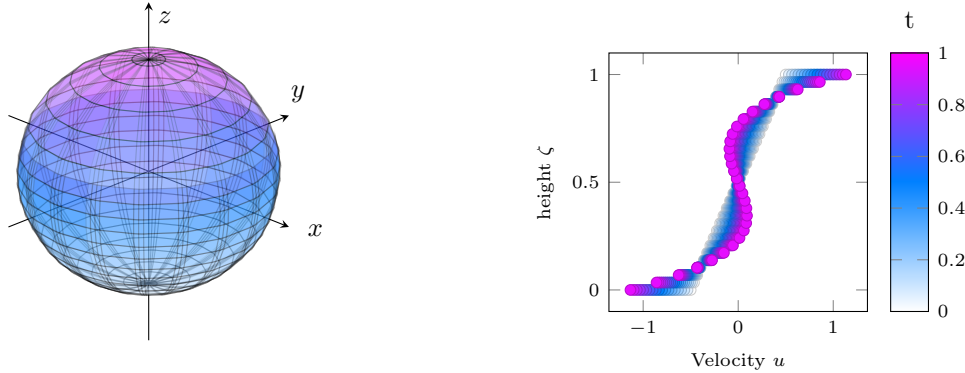
Figure 1b displays 20 samples from a dataset of  $n$  sampled velocity profiles  $u_{t_i}(\zeta)$  evaluated over a 30-point grid  $\zeta_j \in [0, 1]$  on vertical axis  $\forall i \in \{1, \dots, n\}$ . Although each sample appears as a point in 30D space (one feature per grid evaluation), the underlying generative process is governed by a low-dimensional parameterization:

$$t \mapsto u(\zeta)_t = -\frac{1}{2}\tilde{P}_1(\zeta) - \frac{t}{30}\tilde{P}_3(\zeta), \quad \forall t \in [0, 1], \quad (1)$$

where  $\tilde{P}_n(\zeta)$  denotes the scaled Legendre polynomial of degree  $n$  as defined in Kowalski and Torrilhon (2019). If the model can learn the single generative parameter  $t$  for each profile, it should, in principle, reconstruct the full 30-dimensional signal with negligible loss, revealing the dataset's intrinsic dimension to be  $d = 1$ . This second example is of particular interest, as it closely

\*Corresponding author

*Email addresses:* antoine.oriou@student-cs.fr (Antoine Oriou), philipp.krah@cea.fr (Philipp Krah), julian.koellermeier@ugent.be (Julian Koellermeier)



(a) 2-dimensional sphere embedded in 3-dimensional space ( $p = 3$  and  $d = 2$ ). (b) 20 samples taken from a 1-intrinsic-dimensional dataset embedded in a 30 dimensional space ( $p = 30$  and  $d = 1$ ).

Figure 1: Example datasets where the intrinsic dimension of the sampling space differs from its embedded dimension.

resembles our target application: the analysis of velocity profiles of the numerical solution of vertically resolved one-dimensional free-surface flow, see Kowalski and Torrilhon (2019).

Intrinsic dimension estimation methods have been widely used in different fields such as biology (Way et al. (2020)), finance (Sirignano (2016)), and physics (Lee and Carlberg (2019)). Our application addresses the efficient numerical solution of a vertically resolved one-dimensional free-surface flow. Similar to the work of Lee and Carlberg (2019), we employ deep learning methods to overcome the loss of accuracy inherent in linear model reduction techniques such as Proper Orthogonal Decomposition (POD).

Over the years, numerous methods have been proposed to estimate the intrinsic dimension of data (Campadelli et al. (2015), Binnie et al. (2025)), often classified by the geometric information they exploit: tangential estimators (PCA Fan et al. (2010)) detecting local affine structure, parametric estimators based on dimension-dependent probability distributions (Correlation Integral Grassberger and Procaccia (1983), and topological or metric-based estimators. IDEA differs from these approaches by enabling (in addition to the estimation of  $d$ ) the reconstruction of the data after the compression in a  $d$ -dimensional space. It leverages a flexible implementation of controlled sparsity in a neural network double CancelOut layer, adapted from Borisov et al. (2019). Our main contribution lies in the loss function and training procedure, which enforce strong regularization and enable intrinsic dimension estimation through the latent space. Common challenges for such estimators include sensitivity to hyperparameters, large sample requirements, poor performance in high dimensions, and difficulty handling non-linear geometries (Campadelli et al. (2015)). Unlike classical methods, IDEA addresses many of these limitations and does not suffer from explicit weakness. It only requires a sufficiently large sample size, owing to its data-driven nature and reconstruction

capabilities.

The rest of the paper is organized as follows. In Section 2, we explain the structure of IDEA, detailing the training loop and the latent space regularization process. In Section 3, we assess the performance of IDEA on synthetic data. In Section 4, we compare IDEA with other estimators on benchmark datasets from Campadelli et al. (2015). Finally, in Section 5, we apply IDEA to numerical data stemming from one-dimensional free-surface flow simulations from Kowalski and Torrilhon (2019) and showcase the efficiency of our approach to reduce high-dimensional data from numerical solutions to their intrinsic dimension. The paper ends with concluding remarks.

## 2. Mathematical background

### 2.1. Autoencoder neural network

An autoencoder Rumelhart et al. (1986) is a function that aims to compress and reconstruct an input while minimizing the reconstruction error. It has been widely used for diverse machine learning tasks such as image segmentation, classification, and time series predictions, among others Michelucci (2022). An autoencoder is typically divided into three parts: *encoder*, *bottleneck*, and *decoder*. The *encoder* is a function  $f_\theta : \mathbb{R}^p \rightarrow \mathbb{R}^l$ , with  $l \ll p$ , which maps the input data to a lower-dimensional latent space, the *bottleneck*. The *decoder* is a function  $g_\phi : \mathbb{R}^l \rightarrow \mathbb{R}^p$ , which reconstructs the input from the latent representation.

In the context of intrinsic dimension estimation, the structure of the latent space  $\mathbb{R}^l$  plays a central role, as it provides an upper bound of the ID under sufficient reconstruction precision.

### 2.2. Structure of the model

We introduce the Intrinsic Dimension Estimating Autoencoder (IDEA), a neural network autoencoder

specialized for intrinsic dimension estimation (see Goodfellow et al. (2016) for details about neural network implementations).

IDEA’s encoder and decoder are each composed of five fully connected linear layers that map the input to the latent space and vice versa (see Fig. 2). Each layer (except the last) is followed by a normalization layer and a SiLU activation function (respectively introduced in Ba et al. (2016) and Elfwing et al. (2017)).

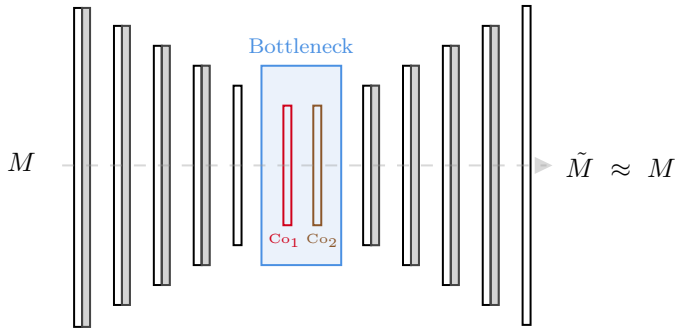


Figure 2: IDEA’s architecture consisting of an encoder, a re-weighted double CancelOut (Co) bottleneck, and a decoder. Grey rectangles represent a block composed of a normalization layer followed by a SiLU activation. The layer sizes are set as follows:  $128 \rightarrow 64 \rightarrow 32 \rightarrow 16 \rightarrow l \rightarrow l \rightarrow 16 \rightarrow 32 \rightarrow 64 \rightarrow 128$ .

To promote dimensionality reduction, the latent space is structured to encourage the elimination of redundant variables. A key component enabling this is the CancelOut layer, here adapted from Borisov et al. (2019). This specialized neural network layer selects a subset of informative latent variables by suppressing those that do not contribute meaningfully to the reconstruction (see Figure 3). Given the central role of the CancelOut layer in our architecture, we provide detailed implementation insights in the following Section 2.3.

### 2.3. Re-weighted double CancelOut layers

Formally, we refer to the bottleneck component as the *Re-weighted Double CancelOut Layer* as we constructed the bottleneck as a superposition of two CancelOut layers with distinct objectives to facilitate the regularization process. We begin by briefly recalling the functioning of the CancelOut layer.

The CancelOut operation is defined as:

$$\text{CancelOut}(X) = X \odot g(W_{\text{CO}}), \quad (2)$$

where  $\odot$  denotes element-wise multiplication,  $X \in \mathbb{R}^l$  is the input vector,  $W_{\text{CO}} \in \mathbb{R}^l$  is a learned weight vector, and  $g$  is an activation function (ReLU) applied element-wise.

The CancelOut layer operation consists of a one-to-one mapping between the input latent variables and the output (See Fig. 3), where each input dimension is multiplied by

a trainable scalar weight.

As each output variable depends only on the corresponding input variable (i.e., the one-to-one mapping ensures no mixing of information across dimensions), setting the  $i^{\text{th}}$  weight to zero completely suppresses the  $i^{\text{th}}$  latent variable. As a result, the corresponding dimension of the latent representation becomes inactive and no longer contributes to the reconstruction.

The CancelOut mechanism provides a direct and controllable path to reduce the effective dimension of the latent space: as training progresses, the model may learn to suppress uninformative or redundant latent variables. The CancelOut Layer thus acts as a sparsity-inducing gate. Formally, the bottleneck of IDEA consists of two successive CancelOut Layers, each with  $l$  neurons (i.e.,  $l$  initially non-negative weights), connected in a one-to-one fashion (see Figure 3).

The first CancelOut layer ( $\text{Co}_1$ ) serves as a sparsity-inducing gate: it is subject to regularization (e.g., L1), which encourages some of its weights to approach zero. This effectively removes certain latent dimensions from contributing to the output, enabling the network to learn the intrinsic dimensionality of the data. The second CancelOut Layer ( $\text{Co}_2$ ) is also a one-to-one mapping, but it is not regularized. Its purpose is to rescale all informative features to a comparable level after the bottleneck, thereby compensating for the magnitude suppression caused by continued regularization of relevant weights.

#### Re-weighted double CancelOut layers

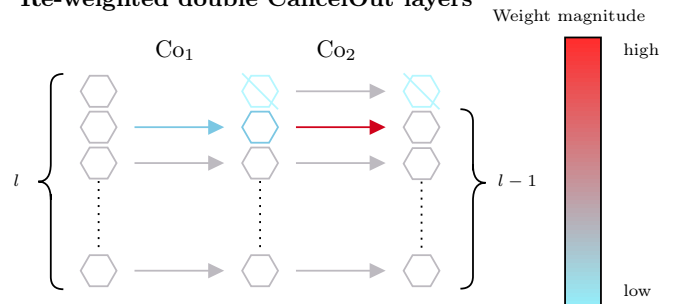


Figure 3: Re-weighted double CancelOut (Co) layers forming the bottleneck. The initial latent dimension is  $l$ . Weights are represented as arrows, variables as hexagons.  $\text{Co}_1$  sets the last weight to zero, effectively removing one dimension from the latent space, while also beginning to regularize the current last non-zero weight (blue), diminishing the magnitude of the corresponding latent variable. In response,  $\text{Co}_2$  increases its corresponding weight (red) to ensure that the remaining  $l - 1$  variables stay on a comparable scale after the bottleneck. In the diagram, the weight regularization process unfolds from top to bottom.

Let  $l_{\text{eff}}$  be the number of effective variables in the latent space (number of non-zero weights of  $\text{Co}_1$ ). If the model can successfully reconstruct the data using a bottleneck with  $l_{\text{eff}}$  effective variables, this implies that the intrinsic dimension is at most  $l_{\text{eff}}$ . Our objective is therefore to encourage the model to minimize the effective dimensionality  $l_{\text{eff}}$  of the bottleneck as much as possible so that it converges towards the smallest  $l_{\text{eff}}$  preserving

reconstruction quality, which is the intrinsic dimension  $d$  of the dataset. This is achieved through the design of the model’s loss function.

#### 2.4. Training loop and detailed loss function

The training loop of our model is its main distinctive feature. We introduce a versatile loss function with specific terms giving the model a simple, but flexible incentive to detect the smallest  $l_{\text{eff}}$  of the dataset via regularization. This consists in adding a penalty term of the weights directly in the loss function Kukačka et al. (2017).

The regularized model is designed to reconstruct the input with the smallest  $l_{\text{eff}}$  preserving reconstruction quality, which is  $d$  by definition. As  $l_{\text{eff}}$  is the number of non-zero weights of  $\text{Co}_1$  (see Section 2.3), we want the loss function (Eq. (3)) to drive the  $\text{Co}_1$  weights toward sparsity by promoting zero-valued entries, while keeping a good overall reconstruction loss. The loss function is

$$\mathcal{L}_{\text{total}} = \underbrace{\mathcal{L}_{\text{rec}}(\hat{x}, x)}_{\text{reconstruction}} + \underbrace{\lambda_{\text{rec}} \cdot \mathcal{L}_{\text{rec}}(\hat{x}_{\text{adj}}, x)}_{\text{projected reconstruction}} + \underbrace{\lambda_{\text{reg}} \cdot \mathcal{L}_{\text{reg}}(w_{\text{co}_1}^{(\text{last})}, \alpha)}_{\text{L1 regularization}} + \underbrace{\lambda_{\text{orth}} \cdot \mathcal{L}_{\text{orth}}(f_{\theta}(x))}_{\text{orthogonality penalty}}, \quad (3)$$

where

- $\hat{x} = g_{\phi}(f_{\theta}(x))$  is the main model output (full reconstruction).
- $\mathcal{L}_{\text{rec}}$  is the MSE reconstruction loss.
- $w_{\text{co}_1}^{(\text{last})}$  is the last non-zero weight in the  $\text{Co}_1$  layer.
- $\lambda_{\text{rec}}, \lambda_{\text{reg}}, \lambda_{\text{orth}}$  are weighting coefficients for projected reconstruction, regularization, and orthogonality penalty, respectively.
- $\hat{x}_{\text{adj}}, \mathcal{L}_{\text{reg}}, \alpha$ , and  $\mathcal{L}_{\text{orth}}$  are detailed below.

*Projected reconstruction:*  $\hat{x}_{\text{adj}}$ . This is the output of the model after setting the last non-zero weight of the  $\text{Co}_1$  layer to zero.  $\hat{x}_{\text{adj}}$  is thus the reconstructed input after compression in an  $l_{\text{eff}} - 1$  dimensional space.

While trying to reduce the reconstruction loss using  $l_{\text{eff}}$  dimensions, the model also attempts to reduce the *projected reconstruction loss*  $\lambda_{\text{rec}} \cdot \mathcal{L}_{\text{rec}}(\hat{x}_{\text{adj}}, x)$ , which is the loss criterion ( $\mathcal{L}_{\text{rec}}$ ) applied to  $\hat{x}_{\text{adj}}$  and scaled by  $\lambda_{\text{rec}}$ . We call it projected because this term anticipates the structure that the model will have if it decides to eliminate a dimension by setting the current  $w_{\text{co}_1}^{(\text{last})}$  to zero.

The elimination of a latent dimension thus consists in a trade-off between the first two terms of the loss function, reflecting the reconstruction error with and without the current last latent dimension, guided by the regularization term.

*L1 regularization:*  $\mathcal{L}_{\text{reg}}, \alpha$ . For the model to understand that it has to reduce  $l_{\text{eff}}$ , we have to attribute a *cost* to each dimension. This is done through the L1 regularization loss

$$\mathcal{L}_{\text{reg}}(w_{\text{co}_1}^{(\text{last})}, \alpha) = \left\| w_{\text{co}_1}^{(\text{last})} + \alpha \right\|_1. \quad (4)$$

With this regularization loss, the model is guided to minimize the L1 norm of  $w_{\text{co}_1}^{(\text{last})}$ . Note that we add a small  $\alpha \ll 1$ , which pushes the model to attribute to the unused weights the value  $-\alpha$ . Since  $\text{Co}_1$  weights are passed through ReLU activation, we ensure that the gradient and the value are nullified after the weight is set to  $-\alpha$ .

*Orthogonality penalty:*  $\mathcal{L}_{\text{orth}}(f_{\theta}(x))$ . This loss is related to latent disentanglement Cha and Thiyagalingam (2022). Its objective is to render the latent space features to become uncorrelated of one another. This leads to learning more generalizable representations of the data and provides a more interpretable set of features, crucial for analysis.

Given a latent representation matrix  $f_{\theta}(x) \in \mathbb{R}^{n \times l}$ , where  $n$  is the number of samples and  $l$  is the latent dimension, we define the orthogonal loss as

$$\mathcal{L}_{\text{orth}}(f_{\theta}(x)) = \left\| C_{f_{\theta}(x)} - I \right\|_F^2, \quad (5)$$

where  $I \in \mathcal{M}_{l \times l}$  is the identity matrix,  $C_{f_{\theta}(x)} \in \mathcal{M}_{l \times l}$  is the correlation matrix of the latent representation  $f_{\theta}(x)$  and  $\|\cdot\|_F^2$  denotes the squared Frobenius norm.

Note that the loss function (3) is evaluated for each batch of input, after which its gradient is computed and the optimizer performs a step towards the minimum of (3). We will evaluate that model in the next parts in a variety of datasets with various intrinsic dimensions and relationships between features.

To assess the reconstruction accuracy of our model, we define the test loss function, which is applied to a held-out subset of the data not used during training. The test loss is given by

$$\mathcal{L}_{\text{test}} = \mathcal{L}_{\text{rec}}(\hat{x}, x), \quad (6)$$

where  $\mathcal{L}_{\text{rec}}, \hat{x}$ , and  $x$  were defined in the context of the training loss function above.

Finally, Table 1 states the hyperparameters chosen for our model. We chose a set of hyperparameters with the intention to keep them constant for all applications of our model, because one of our objectives is the versatility and adaptability of the model on different structures. We will only change the sample size when necessary to allow the model to learn particularly difficult structures within a time unnecessary for simpler datasets. In the following sections, we denote by  $\tilde{d}$  the predicted value of  $d$ , the intrinsic dimension of the dataset. By definition,  $\tilde{d}$  corresponds to the number of non-zero weights in  $\text{Co}_1$ , denoted as  $l_{\text{eff}}$ , after the completion of training.

Table 1: Hyperparameters selected for the model.

Hyperparameter	Value
Overall Learning rate	$1 \times 10^{-4}$
Learning rate of $\text{Co}_1$	$2 \times 10^{-4}$
Batch size	256
Number of epochs	Variable
$l$ (initial dimension of the bottleneck)	Variable
Optimizer	Adam
$\lambda_{\text{rec}}$	1
$\lambda_{\text{reg}}$	0.001
$\lambda_{\text{orth}}$	0.001

### 3. Synthetic data tests: Legendre velocity profiles

In this section we evaluate the model on synthetic data. This serves as the first step towards evaluating the model on numerical solutions of vertically resolved one-dimensional free-surface flow, and compare it to the projection of the solution on the scaled Legendre polynomial basis Koellermeier (2021). The synthetic data in this section is thus generated by a random linear combination of scaled Legendre polynomials.

#### 3.1. Dataset generation

We generated 3 different datasets with different number of intrinsic dimension ( $d$ ) as follows:

Let  $\zeta \in [0, 1]$  be discretized over a grid of size  $N_\zeta = 100$ , and let  $P_k(\zeta)$  denote the  $k$ -th scaled Legendre polynomial, defined in Kowalski and Torrilhon (2019).

The dataset  $\{f^{(j)}(\zeta)\}_{j=1}^n$  is constructed using

$$f^{(j)}(\zeta) = P_1(\zeta) + \sum_{k \in \mathcal{S}} \alpha_k^{(j)} P_k(\zeta), \quad (7)$$

where  $\alpha_k^{(j)} \sim \mathcal{U}(0, 1)$  are i.i.d. uniform random variables for each sample  $j \in \{1, \dots, n\}$ ,  $n$  being the number of samples.

The set of polynomials  $\mathcal{S} \in \mathcal{P}(\mathbb{N})$  is predefined for each of the three datasets generated. As each random variable  $\alpha_k$  is independent from the others, each one contributes to one independent dimension, thus we have the intrinsic dimension  $d = |\mathcal{S}|$ .

We generate datasets of size  $n = 20,000$  of the intrinsic dimensions given in Table 2.

Table 2: Summary of synthetic dataset characteristics and IDEA reconstruction errors (mean squared error).

#	$\mathcal{S}$	$d$	$\tilde{d}$	$\mathcal{L}_{\text{test}}$		
				$\tilde{d}+1$	$\tilde{d}$	$\tilde{d}-1$
1	{3}	1	1	$7.3 \cdot 10^{-7}$	$7.8 \cdot 10^{-7}$	$1.28 \cdot 10^{-2}$
2	{3, 5}	2	2	$1.3 \cdot 10^{-6}$	$1.5 \cdot 10^{-6}$	$2.0 \cdot 10^{-3}$
3	{3, 5, 6, 7}	4	4	$9.6 \cdot 10^{-6}$	$9.7 \cdot 10^{-6}$	$1.3 \cdot 10^{-3}$

All instances of the models were initialized with a latent size  $l = 8$ . For these three datasets, IDEA successfully predicted the correct intrinsic dimension  $\tilde{d} = d$  as shown in Table 2. Note that since the polynomials are evaluated on a 100-point grid, the embedded dimension is  $p = 100$  here.

#### 3.2. Model performance

A distinctive feature of our model is that it does not only successfully predict the intrinsic dimension, but it also reconstructs the data. In fact, when the model estimates a specific dimension  $\tilde{d}$ , the training loop outputs the best model with  $\tilde{d} - 1$ ,  $\tilde{d}$  and  $\tilde{d} + 1$ . For the synthetic data test case, this leads to the results shown in Table 2.

The results in table (2) show that the predicted intrinsic dimension  $\tilde{d}$  is indeed correct, as a reconstruction with  $\tilde{d} - 1$  intrinsic variables leads to substantial reconstruction loss, while a reconstruction with  $\tilde{d} + 1$  intrinsic dimensions does not lead to an additional gain in accuracy.

Figure 4 shows the evolution of the test loss  $\mathcal{L}_{\text{test}}$  during the training on dataset 3. We obtain from the plot that the training can be characterized by two distinct phases:

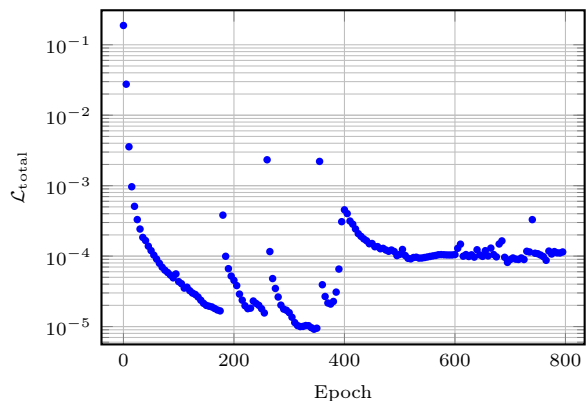


Figure 4: Synthetic dataset 3 total train loss  $\mathcal{L}_{\text{total}}$  as a function of training epoch.

*Phase 1: Epoch 1-500.* In the first phase, the network progressively suppresses non-contributing latent dimensions. Each time one latent variable is eliminated ( $l_{\text{eff}}$  decreases by one), the loss function spikes because the network adjusts the modified loss function.

*Phase 2: Epoch 500-800.* In the last phase, the network stops eliminating dimensions because it no longer considers the trade-off between reconstruction loss and projected reconstruction loss to be interesting. We can see that it is attempting to project the latent space onto 3 dimensions, which appears to be insufficient for accurate reconstruction. The test loss oscillates around its local minimum.

### 3.3. Latent space disentanglement

We added a term for latent disentanglement  $\mathcal{L}_{\text{orth}}$  in the training loss function Eq. (3), promoting zero Pearson correlation among latent variables. After training, by computing the latent representation of the data ( $f_{\theta}(x)$ ), we can plot a correlation matrix of the latent representation. We will also observe the correlation between the latent variables  $L_i$ , for  $i = 0, \dots, \tilde{d} - 1$  learned by the model and the original coefficient  $\alpha_i$ , for  $i \in S$  in front of each polynomial (generated by uniform distribution) from Eq. (7).

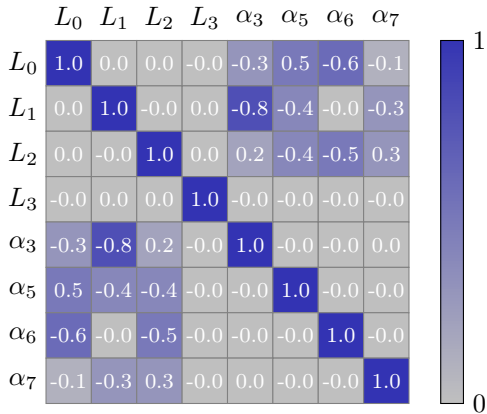


Figure 5: Correlation matrix of dataset 3, between the four latent variables  $L_i$  and the projection coefficients on the scaled Legendre polynomial basis  $\alpha_i$  (Eq. (7)). The color varies according to the absolute value of the correlation between the parameters.

We can see in Figure 5 that even though the latent space is completely uncorrelated and so are the  $\alpha_i$ 's, the model learns a combination of coefficients, making it difficult to link the latent variables of the model to the coefficients of the orthogonal projection. We note that while  $L_3$  is almost uncorrelated with the  $\alpha_i$ , it still encodes information about them, as shown in Table 2, where the reconstruction without  $L_3$  yields a much higher test loss. We recall that Pearson correlation captures only linear relationships; thus, a correlation of zero does not imply independence, but may instead indicate the presence of nonlinear dependencies.

After the successful synthetic data tests, we continue with benchmark tests.

## 4. Benchmark tests: structured manifolds

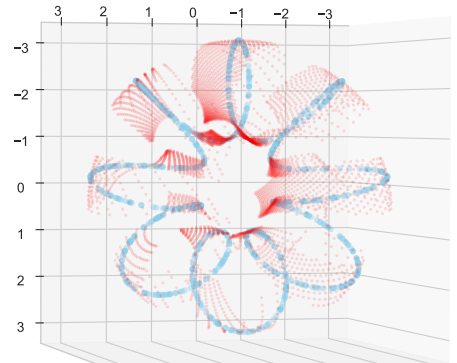
### 4.1. Choice of dataset and benchmark comparison

We perform a comparative evaluation of our model with the benchmark framework applied to relevant state-of-the-art intrinsic dimension estimators presented in Campadelli et al. (2015). The model is evaluated on synthetic datasets provided by the module `scikit-dimension` presented in Bac et al. (2021) which reuses those from Campadelli et al. (2015). The synthetic datasets are generated by drawing

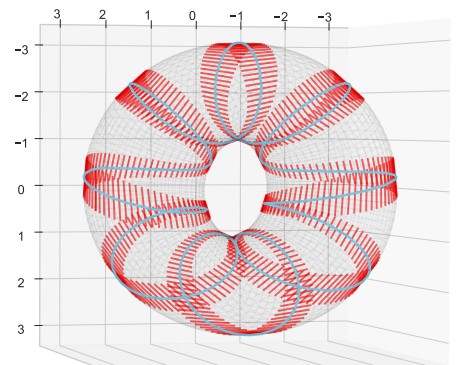
samples from manifolds ( $\mathcal{M}$ ) linearly or nonlinearly embedded in higher-dimensional spaces, see Table 3. The original paper did not evaluate the estimators on  $\mathcal{M}_{5a}$ . For this dataset, we reproduced the estimation using the same parameters to report the results. `TwoNN` and `1PCA` are not reported in Campadelli et al. (2015), we used the default hyperparameters from `scikit-dimension`.

As shown in Table 3, IDEA accurately predicts the intrinsic dimension of the datasets. While baseline estimators can have blind spots on specific datasets, leading to significant estimation errors, IDEA consistently approximates the true intrinsic dimension on all of these datasets. We note that for complex nonlinear manifolds, a larger number of samples was sometimes required to achieve accurate prediction. This led to increased computation time (see Appendix A, where we illustrate how prediction accuracy evolves with sample size).

As our model is able to reconstruct the dataset under the estimated dimension, we can also compute reconstruction losses, see Appendix A.



(a) Representation of the one-dimensional helix dataset (sky blue) and model's reconstruction of the complete latent space with  $l_{\text{eff}} = 2$  (red).



(b) Theoretical representation of the input dataset (sky blue), the manifold in which IDEA projected the data (red), and the subspace of the known two-dimensional manifold torus (light grey).

Figure 6: Representations of the estimated latent space of IDEA upon the one-dimensional helix ( $\mathcal{M}_{5a}$ ) (a) and the theoretical manifold from which it is taken (b).

Table 3: Benchmark datasets characteristics (intrinsic dimension  $d$  and embedded dimension  $p$ ), and result comparison of the intrinsic dimension estimation  $\tilde{d}$  between IDEA and state-of-the-art from Campadelli et al. (2015) including new benchmark dataset of embedded helix ( $\mathcal{M}_{5a}$ ). Green cells denote an exact estimation (within  $d \pm 0.05$ ), whereas cells in red indicate an error exceeding one dimension from the true value.

Name	Description	$d$	$p$	IDEA	MLE	TwoNN	CD	MIND <sub>KL</sub>	DANCo	1PCA
$\mathcal{M}_1$	10D sphere linearly embedded	10	11	10.0	9.10	9.97	9.12	10.30	10.09	11.00
$\mathcal{M}_2$	Affine space	3	5	3.0	2.88	2.98	2.88	3.00	3.00	3.00
$\mathcal{M}_3$	Concentrated figure, mistakable with a 3D one	4	6	5.0	3.83	3.77	3.23	4.00	4.00	5.00
$\mathcal{M}_4$	Nonlinear manifold	4	8	4.0	3.95	3.80	3.88	4.15	4.00	8.00
$\mathcal{M}_{5b}$	2D helical surface embedded in 3D	2	3	2.0	1.97	2.02	1.98	2.00	2.00	3.00
$\mathcal{M}_6$	Nonlinear manifold	6	36	6.0	6.39	5.86	5.91	6.50	7.00	12.00
$\mathcal{M}_7$	Swiss Roll	2	3	2.0	1.96	2.00	1.93	2.07	2.00	3.00
$\mathcal{M}_{Beta}$	sample of $N$ points in $[0, 1]^{10}$ , according to a beta distribution $\beta_{0.5, 10}$ ,	10	40	10.0	6.36	6.77	3.05	7.00	7.00	10.00
$\mathcal{M}_{P3}$	3D paraboloid, nonlinearly embedded according to a multivariate Burr distribution ( $\alpha = 1$ )	3	12	3.0	2.89	2.98	2.43	3.00	3.00	1.00
$\mathcal{M}_{P6}$	6D paraboloid, nonlinearly embedded according to a multivariate Burr distribution ( $\alpha = 1$ )	6	21	6.0	4.96	5.44	3.58	5.04	6.00	1.00
$\mathcal{M}_{5a}$	1D helix embedded in 3D	1	3	2.0	1.06	0.99	1.00	1.00	1.00	3.00

#### 4.2. Analyzing nonlinear reconstruction and possible improvements

IDEA exhibited difficulties with the one-dimensional helix  $\mathcal{M}_{5a}$ , a complex nonlinear helix embedded in a 3D space. IDEA predicted an intrinsic dimension  $\tilde{d} = 2$  for this one-dimensional manifold. By evaluating the decoder on a grid of points spanning the latent space, we observed (Fig. 6) that IDEA identified a manifold  $\mathcal{S}_{\mathcal{T}}$  that can be mapped into  $\mathbb{R}^2$  and contains the helix ( $\mathcal{H}_1$ ). Geometrically,  $\mathcal{S}_{\mathcal{T}}$  resembles a ribbon surrounding the two-dimensional torus along the poloidal direction. Formally, a topological manifold of dimension  $d$  is a topological space  $M$  such that every point  $p \in M$  has a neighborhood  $U$  homeomorphic to an open subset of  $\mathbb{R}^d$ . This condition holds for the torus, and here the data-oriented “intrinsic dimension” coincides with the topological dimension of the projected space, namely 2. IDEA found a manifold  $\mathcal{S}_{\mathcal{T}}$  of dimension less than  $p$  which contains the data. However, this manifold  $\mathcal{S}_{\mathcal{T}}$  does not align with the neighborhood structure of  $\mathcal{H}_1$  which is in fact a one-dimensional manifold.

While the performance of IDEA is very good also in comparison with the state-of-the-art, several strategies could be investigated to further improve the model’s performance on special nonlinear manifolds, provided that the potential increase in computation time is acceptable: First, the model exhibits significant sensitivity to the learning rate of the bottleneck layer weights, which is currently set to  $2 \cdot 10^{-4}$ , while the global learning rate is fixed at  $1 \cdot 10^{-4}$ . To better adapt to the characteristics of each dataset, we propose the integration of more advanced learning rate tuning techniques such as learning

rate warm-up Kalra and Barkeshli (2024), learning rate scheduling (we currently employ a StepLR scheduler with `step = 400`), and cyclical learning rates Smith (2017). These approaches could increase the model’s flexibility by allowing the learning rate to adapt dynamically during training, thus reducing the need for manual tuning. Second, the current disentanglement procedure is based on the Pearson correlation coefficient, which is limited to detecting linear dependencies between latent variables. To capture a broader class of relationships, we suggest replacing or complementing this metric with more general dependence measures such as the  $\chi$ -correlation coefficient Chatterjee (2020) or mutual information Carrara and Ernst (2019), which are capable of capturing both linear and nonlinear associations. These methods could promote both a more expressive and more interpretable latent representation, though at the cost of higher computational resources.

## 5. Application test: vertically resolved free-surface flow

### 5.1. Reference system and data generation

Shallow flow models are widely used in applications such as weather forecasting and simulation-based natural hazard assessment Kowalski and Torrilhon (2019). Our application case considers a vertically resolved one-dimensional free-surface shallow flow PDE model, which describes the evolution of the vertical velocity profile  $u(t, x, \zeta)$  and the free-surface height  $h(t, x)$  over time  $t$  and along the  $x$  axis, where  $\zeta \in [0, 1]$  denotes a normalized

vertical coordinate.

According to Kowalski and Torrilhon (2019), The governing equations are

$$\partial_t h + \partial_x(hu) + \partial_\zeta(h\omega) = 0, \quad (8)$$

$$\partial_t(hu) + \partial_x\left(hu^2 + \frac{1}{2}h^2\right) + \partial_\zeta(hu\omega) = \frac{R}{h}\partial_\zeta\zeta u, \quad (9)$$

subject to the boundary conditions

$$\partial_\zeta u|_{\zeta=0} = \frac{h}{\chi}u|_{\zeta=0}, \quad \partial_\zeta u|_{\zeta=1} = 0. \quad (10)$$

The initial condition of a smooth wave is given by:

$$h(x, 0) = 1 + \exp(3 \cos(\pi(x + x_0)) - 4), \quad (11)$$

where  $\omega(t, x, \zeta)$  is a vertical velocity coupling term,  $R$  is the friction coefficient and  $\chi$  is the slip length. We refer to Kowalski and Torrilhon (2019) for more details.

While the reference system from Kowalski and Torrilhon (2019) can be discretized pointwise in the  $\zeta$  direction, often only a few macroscopic variables can describe the full vertical velocity profile, in which case their number corresponds to the ID of the profiles. One example is the vertical average  $u_m(t, x)$ , which could be computed purely from the reduced, so-called shallow water equations. However, such simple models often fail to capture important vertical dynamics in realistic settings Koellermeier (2021).

More accurate models, such as the moment approximation presented in Kowalski and Torrilhon (2019), project the reference solution onto a subset  $\mathcal{S}$  of the scaled Legendre polynomial basis, yielding coordinates (also called moments)  $\alpha_i$  for each  $i \in \mathcal{S}$ . However, such models may use more parameters than the intrinsic dimension of the profile, which is expected to lie on a 2-dimensional manifold (along  $x$  and  $t$ ).

To address this limitation, we propose using IDEA to learn a compact and informative latent representation of the vertical velocity profile. Specifically, we apply our model to data generated from a pointwise numerical discretization of the vertically resolved system, on a grid of size  $n_t \times n_x \times n_\zeta$ , as in Kowalski and Torrilhon (2019). The resulting solution is transformed into a dataset represented as a matrix  $M \in \mathcal{M}_{n_x \cdot n_t, n_\zeta + 1}(\mathbb{R})$ . The first column of the dataset is the water height  $h(x_i, t_i)$  evaluated for each point of the grid along  $x$  and  $t$ . IDEA successfully balances computational efficiency and reconstruction accuracy by learning a precise mapping of the full solution into a lower-dimensional latent space of size  $1 < d < n_\zeta$ , thus identifying the ID of the velocity profiles.

## 5.2. Model specifications for application to free-surface flows

The objective is to reduce the dimensionality of the velocity profile space, using our intrinsic estimator model IDEA. As each point has one water height feature, we explicitly reserve one latent dimension for representing the water height, and encourage the model to learn this value by adding a term in the loss function ( $\mathcal{L}_h$ ) which penalizes how far the first latent variable ( $L_0$ , first coordinate of the output vector of the layer Co2) deviates from  $h(x, t)$  using the MSE.

The loss function therefore reads

$$\mathcal{L}_{\text{SWE}} = \underbrace{\mathcal{L}_{\text{total}}(\hat{x}, x, \hat{x}_{\text{adj}}, w_{\text{co1}}^{\text{(last)}})}_{\text{initial loss}} + \underbrace{\mathcal{L}_h(L_0, h(x, t))}_{\text{Water height Loss}}, \quad (12)$$

where  $\mathcal{L}_{\text{total}}$  is the loss previously defined, and  $\mathcal{L}_h$  is the additional loss for the deviation of the first latent variable from the water height.

## 5.3. Results and reconstruction analysis

We consider two cases.

### 5.3.1. First case: simple solution with a small number of moments ( $\mathcal{M}_1$ )

IDEA is first evaluated on a solution that can be accurately reconstructed using only a few moments. By setting a large slip length  $\chi = 10^6$ , we eliminate bottom friction entirely, allowing the profile to evolve more freely and preserve a structure that stabilizes quickly. Fig. 7 shows that from time  $t \approx 0.3$ , the only significant moments are  $\alpha_0$ ,  $\alpha_1$  and  $\alpha_3$ . IDEA is then applied to the data generated by the reference solution for  $t \in [0.3, 1]$ , starting with  $l_{\text{eff}} = 8$ . The corresponding results are presented in Table 4.

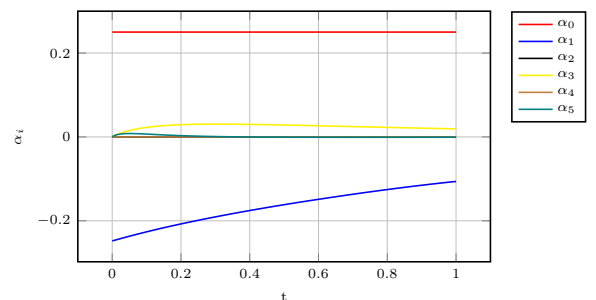


Figure 7: Free-surface flow: data evolution with time of the 6 first projection coefficient  $\alpha_i$ , averaged along  $x$

As observed in Table 4, IDEA predicts  $\tilde{d} = 3$  intrinsic dimensions, including one latent variable for the water height. This correctly suggests that the velocity profiles lie on a 2-dimensional manifold, as expected. Fig. 8 presents the correlation between the 2-dimensional mapping of the full solution and the projection coefficient of the velocity profiles on the scaled Legendre basis computed  $\forall x, t$ .

Table 4: Summary of reconstruction error across application test datasets and the projected dimensions.

Dataset	$d$	$\tilde{d}$	$l$	$t_0$	# Epochs	# Samples	$\mathcal{L}_{\text{test}}$		
							$\tilde{d} + 1$	$\tilde{d}$	$\tilde{d} - 1$
$\mathcal{M}_1$	3	3	8	0.3	1000	24600	$3.50 \times 10^{-6}$	$6.36 \times 10^{-6}$	$4.16 \times 10^{-5}$
$\mathcal{M}_2$	3	3	8	0.1	2000	75300	$1.13 \times 10^{-5}$	$4.31 \times 10^{-6}$	$4.62 \times 10^{-5}$

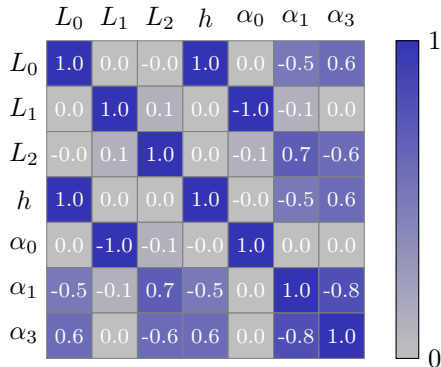


Figure 8: Pearson correlation matrix between the three latent variables  $L_i$  and the coefficients  $a_i$ . The color varies according to the absolute value of the correlation between the parameters.

As expected, the first latent variable is perfectly correlated with the water height  $h$ . Furthermore,  $L_1$  is perfectly negatively correlated with  $\alpha_0$  and  $L_2$  is a combination of  $\alpha_1$  and  $\alpha_3$ . The correlation between  $\alpha_1$  and  $\alpha_3$  is captured by our model. IDEA needs only one variable to simulate the action of  $\alpha_1$  and  $\alpha_3$ , whereas a moment model would need both projection coefficients. This means that IDEA indicates the possibility of a more efficient representation using a non-linear ansatz.

Fig. 9 depicts the relative  $L_2$  loss of the projection of the reference solution on a subset  $\mathcal{S}_n = \{P_1, \dots, P_n\}$  of the scaled Legendre polynomial basis. This truncation loss is compared with the loss of IDEA on the test set. We see that for  $\mathcal{M}_1$ , 4 moments are necessary to make the projection more accurate than the 2-dimensional mapping of IDEA. This shows that a trivial moment model with dense basis is not efficient in approximating the data, while the sparse representation with only 2 latent variables for the velocity field as computed by IDEA is both accurate and efficient.

Note that the relative  $L_2$  loss is computed as

$$\text{Loss} = \frac{\|X - \tilde{X}\|_F}{\|X\|_F}, \quad (13)$$

where  $X$  is the true dataset,  $\tilde{X}$  is the prediction and  $\|\cdot\|_F$  the Frobenius norm.

### 5.3.2. Second case: complex solution with a large number of moments ( $\mathcal{M}_2$ )

For the second test case, we set  $\chi = 0.01$  and  $R = 0.01$ , these coefficients create velocity profiles with a complex dependency on  $\zeta$ , involving several moments, see Kowalski and Torrilhon (2019). Unlike case 1, the moments do not stabilize and  $|\alpha_i|$  is increasing with time for the majority of moments, meaning that the velocity profile becomes increasingly complex, as shown in Fig. 10.

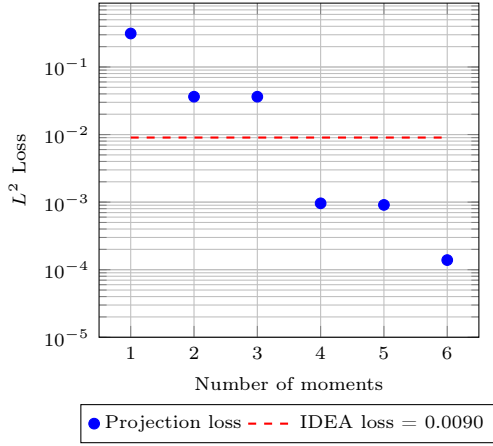
As Table 4 indicates, IDEA predicts an intrinsic dimension  $\tilde{d} = 3$ , including keeping one latent variable for the water height. As expected, the model correctly estimates that these complex velocity profiles lie in a 2-dimensional manifold. This result indicates that while a moment model would need more parameters to describe more complex solutions, IDEA captures underlying dependencies that allow the reconstruction of the profiles using only two dimensions, the correctly estimated intrinsic dimension of the solution.

Correlations are shown in Fig. 11. Consistent with expectations, the first latent variable is perfectly correlated with the water height  $h$ . The two other latent variables now learn a combination of all remaining moments of the solution, leveraging the fact that these moments are correlated. This level of compression is difficult to achieve with traditional moment models, which require more parameters to reach comparable accuracy. In Fig. 9 (b), for example, it is shown that at least 7 coefficients  $\alpha_i$  are necessary to capture the data to a comparable accuracy, while IDEA is able to achieve this accuracy only using 2 latent variables.

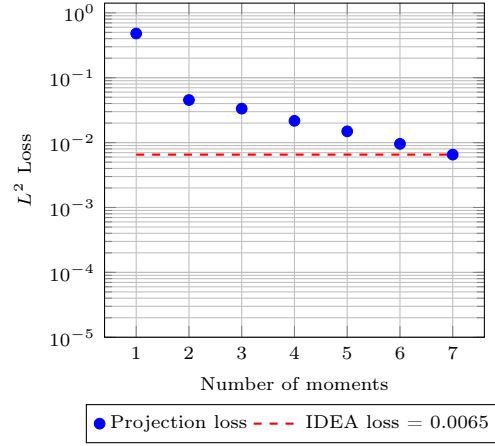
In sum, IDEA successfully predicts the intrinsic dimension of the two application test datasets and succeeds at accurate reconstructions.

## 6. Conclusion

We introduced IDEA, the Intrinsic Dimension Estimating Autoencoder, as a neural network autoencoder model designed to estimate the intrinsic dimension of datasets while preserving strong reconstruction capabilities. By leveraging the flexible architecture offered by the autoencoder architecture and a novel regularization scheme through an innovative use of re-weighted CancelOut layers, IDEA identifies and suppresses redundant latent variables directly within



(a)  $\mathcal{M}_1$  results for the 6 first scaled Legendre polynomials



(b)  $\mathcal{M}_2$  results for the 7 first scaled Legendre polynomials

Figure 9: Comparison of the  $L_2$  loss between the projected solution on a subset of the  $n$  first scaled Legendre polynomials and the  $L_2$  loss of IDEA model on the test set.

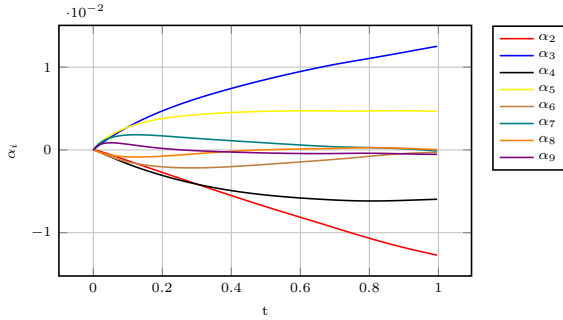


Figure 10: Time evolution of coefficients  $\alpha_i, i = 2, \dots, 9$ , averaged along  $x$ . As  $\alpha_0$  and  $\alpha_1$  are on larger scales, they are excluded from the plot to avoid distortion.

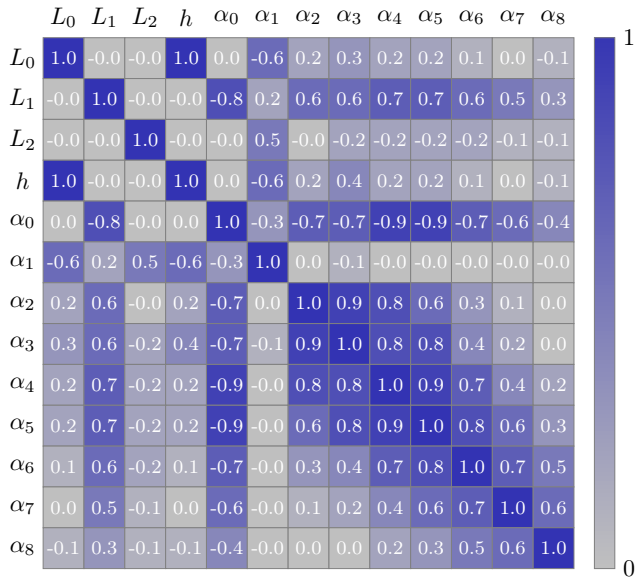


Figure 11: Correlation matrix between the three latent variables  $L_i$  and the coefficients  $a_i$ . The color varies according to the absolute value of the correlation between the parameters.

the network, thanks to a projected loss and latent space disentanglement, effectively identifying dimensional structure underlying the data.

Through a series of synthetic and theoretical benchmarks, IDEA demonstrated competitive performance compared to state-of-the-art intrinsic dimension estimators. Unlike classical estimators, our model directly provides integer-valued intrinsic dimensions by counting active latent variables. This offers an interpretable and adjustable latent space on which analysis can be directly performed, thus enabling more efficient computation. Additionally, IDEA provides a direct reconstruction of the data.

Applying IDEA to a physically motivated case such as the one-dimensional free-surface flow, our model successfully identified a low-dimensional latent representation that preserved the key dynamical structures of the system. We showed that IDEA is a significant advantage over standard moment models, which required a larger number of parameters to capture similar dynamics, due to their limited ability to exploit correlations between higher-order moments.

### Declaration of competing interest

The authors declare that they have no known competing financial interests or personal relationships that could have appeared to influence the work reported in this paper.

### Data and Code availability

The code will be made publicly available on Zenodo in the form of a Jupyter notebook upon acceptance of the manuscript. Prior to publication, it is available from the authors upon reasonable request.

## Author Contribution Statement (CRediT)

**Antoine Oriou:** Conceptualisation, Methodology, Software, Investigation, Numerical Experiments, Writing - Original Draft, Visualisation

**Philipp Krah:** Conceptualisation, Methodology, Writing - Original Draft, Supervision, Writing - Review & Editing

**Julian Koellermeier:** Conceptualisation, Methodology, Writing - Original Draft, Supervision, Writing - Review & Editing

## Acknowledgement

This publication is part of the project *HiWAVE* with file number VI.Vidi.233.066 of the *ENW Vidi* research programme, funded by the *Dutch Research Council (NWO)* and the ANR AAPG 2025 CROKE research grant.

## Appendix A. Model reconstruction and accuracy on benchmark datasets

As our model is able to reconstruct the dataset under the estimated dimension, we can compute reconstruction losses. As stated before, when the predicted dimension is  $\tilde{d}$ , the model keeps track of the best reconstruction estimator with  $\tilde{d} + 1$ ,  $\tilde{d}$  and  $\tilde{d} - 1$  latent dimensions (see benchmark results in Table A.5). We trained the model on all the datasets for a total of 1000 epochs, reserving 20% of the data for testing. The weights of the CancelOut layers were initialized to 1, while all linear layers use PyTorch’s default initialization (Kaiming uniform). The *best model* at each candidate latent dimensionality is selected dynamically during training by monitoring the test reconstruction and projected loss. During training a dictionary of the best states is maintained: It saves the model state for the current  $l_{\text{eff}}$  dimension if its test loss improves. It stores an  $l_{\text{eff}} - 1$  version with the last CancelOut weight forced to zero if this gives a lower projected loss. It prunes states corresponding to dimensions that are  $\geq l_{\text{eff}} + 2$ . This ensures that for every plausible latent dimension  $\tilde{d}$ , we retain the optimal set of parameters found during training.

Figure A.12 shows the evolution of the predicted dimension with the sample size of the dataset.

## Bibliography

Ba, J.L., Kiros, J.R., Hinton, G.E., 2016. Layer normalization. URL: <https://arxiv.org/abs/1607.06450>, arXiv:1607.06450.

Bac, J., Mirkes, E.M., Gorban, A.N., Tyukin, I., Zinovyev, A., 2021. Scikit-dimension: A python package for intrinsic dimension estimation. *Entropy* 23, 1368. URL: <http://dx.doi.org/10.3390/e23101368>, doi:10.3390/e23101368.

Binnie, J.A.D., Dłotko, P., Harvey, J., Malinowski, J., Yim, K.M., 2025. A survey of dimension estimation methods. URL: <https://arxiv.org/abs/2507.13887>, arXiv:2507.13887.

Borisov, V., Haug, J., Kasneci, G., 2019. CancelOut: A Layer for Feature Selection in Deep Neural Networks. pp. 72–83. doi:10.1007/978-3-030-30484-3\_6.

Campadelli, P., Casiraghi, E., Ceruti, C., Rozza, A., 2015. Intrinsic dimension estimation: Relevant techniques and a benchmark framework. *Mathematical Problems in Engineering* 2015, 1–21. doi:10.1155/2015/759567.

Carrara, N., Ernst, J., 2019. On the estimation of mutual information. URL: <https://arxiv.org/abs/1910.00365>, arXiv:1910.00365.

Cha, J., Thiyagalingam, J., 2022. Disentangling autoencoders (dae). URL: <https://arxiv.org/abs/2202.09926>, arXiv:2202.09926.

Chatterjee, S., 2020. A new coefficient of correlation. URL: <https://arxiv.org/abs/1909.10140>, arXiv:1909.10140.

Elfving, S., Uchibe, E., Doya, K., 2017. Sigmoid-weighted linear units for neural network function approximation in reinforcement learning. URL: <https://arxiv.org/abs/1702.03118>, arXiv:1702.03118.

Fan, M., Gu, N., Qiao, H., Zhang, B., 2010. Intrinsic dimension estimation of data by principal component analysis. URL: <https://arxiv.org/abs/1002.2050>, arXiv:1002.2050.

Goodfellow, I., Bengio, Y., Courville, A., 2016. *Deep Learning*. MIT Press. <http://www.deeplearningbook.org>.

Grassberger, P., Procaccia, I., 1983. Measuring the strangeness of strange attractors. *Physica D: Nonlinear Phenomena* 9, 189–208. URL: <https://www.sciencedirect.com/science/article/pii/0167278983902981>, doi:[https://doi.org/10.1016/0167-2789\(83\)90298-1](https://doi.org/10.1016/0167-2789(83)90298-1).

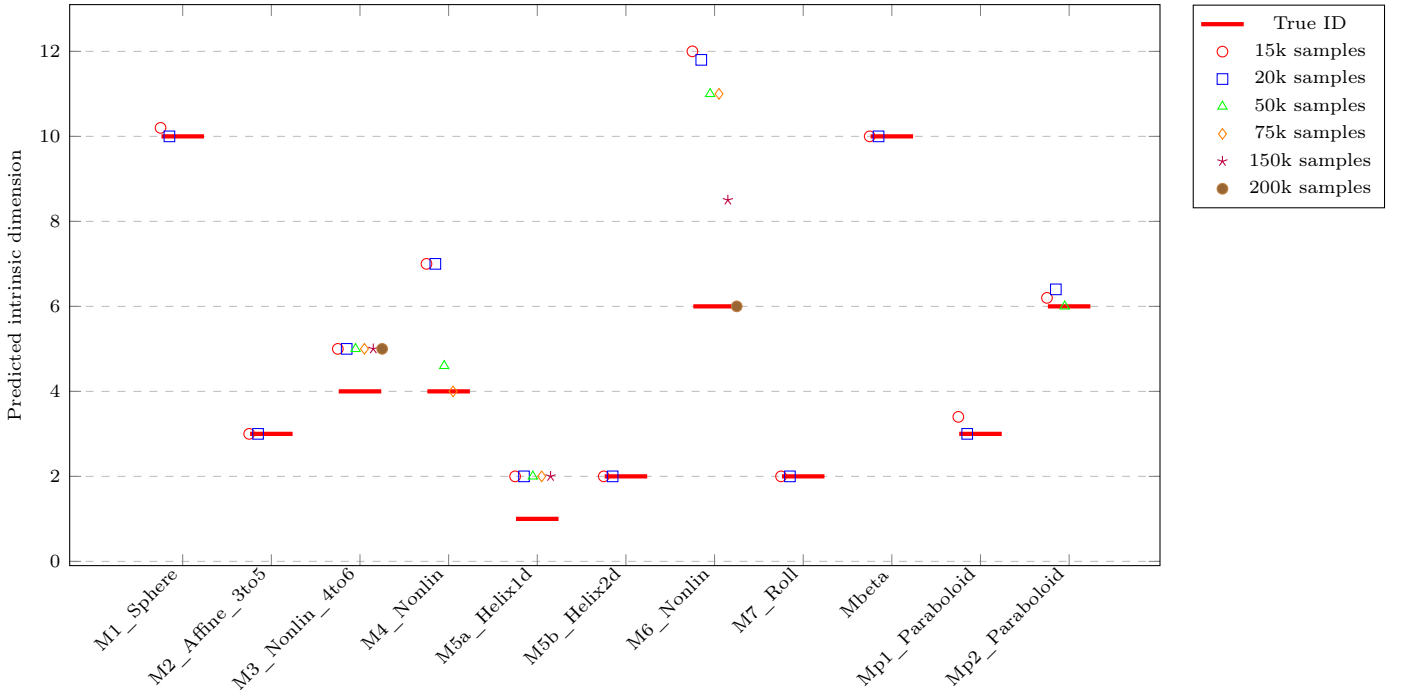
Kalra, D., Barkeshli, M., 2024. Why warmup the learning rate? underlying mechanisms and improvements. doi:10.48550/arXiv.2406.09405.

Koellermeier, J., 2021. Recent developments in modeling free-surface flows with vertically-resolved velocity profiles using moments.

Kowalski, J., Torrilhon, M., 2019. Moment approximations and model cascades for shallow flow. *Communications in Computational Physics* 25. doi:10.4208/cicp.0A-2017-0263.

Table A.5: Summary of reconstruction error across datasets and projected dimensions. We present in this table the most accurate model with the smaller size of dataset.  $l$  is the initial number of non-zero weights of the model. The columns  $\tilde{d}$ , # **Time**,  $\mathcal{L}_{\text{test}}$  are averaged on 5 independent trainings (except for  $\mathcal{M}_6$  which is averaged on 2 independent trainings). Reported computation times correspond to single-thread execution without GPU acceleration.

Dataset	$d$	$\tilde{d}$	$l$	# Samples	# Time	$\mathcal{L}_{\text{test}}$		
						$\tilde{d} + 1$	$\tilde{d}$	$\tilde{d} - 1$
$\mathcal{M}_1$	10	10.0	11	20000	3min51s	$2.9 \times 10^{-4}$	$3.0 \times 10^{-4}$	$4.4 \times 10^{-3}$
$\mathcal{M}_2$	3	3.0	5	15000	1min51s	$5.30 \times 10^{-6}$	$5.31 \times 10^{-6}$	$4.0 \times 10^{-4}$
$\mathcal{M}_3$	4	5.0	6	20000	3min47s	$1.85 \times 10^{-5}$	$1.90 \times 10^{-5}$	$1.0 \times 10^{-4}$
$\mathcal{M}_4$	4	4.0	8	75000	13min37s	$1.87 \times 10^{-4}$	$2.00 \times 10^{-4}$	$5.5 \times 10^{-3}$
$\mathcal{M}_{5a}$	1	2.0	3	20000	3min41s	$3.68 \times 10^{-6}$	$3.85 \times 10^{-6}$	$4.2 \times 10^{-3}$
$\mathcal{M}_{5b}$	2	2.0	3	15000	1min42s	$5.28 \times 10^{-6}$	$5.93 \times 10^{-6}$	$1.69 \times 10^{-2}$
$\mathcal{M}_6$	6	6.0	16	200000	37min06s	$1.10 \times 10^{-4}$	$1.62 \times 10^{-4}$	$7.00 \times 10^{-4}$
$\mathcal{M}_7$	2	2.0	3	15000	2min15s	$4.37 \times 10^{-6}$	$4.37 \times 10^{-6}$	$2.00 \times 10^{-2}$
$\mathcal{M}_{\text{beta}}$	10	10.0	16	15000	3min03s	$9.52 \times 10^{-5}$	$9.54 \times 10^{-5}$	$4.04 \times 10^{-4}$
$\mathcal{M}_{P3}$	3	3.0	12	20000	5min34s	$4.57 \times 10^{-6}$	$4.59 \times 10^{-6}$	$0.80 \times 10^{-4}$
$\mathcal{M}_{P6}$	6	6.0	16	50000	10min36s	$1.57 \times 10^{-5}$	$1.57 \times 10^{-5}$	$0.30 \times 10^{-4}$



- Kukačka, J., Golkov, V., Cremers, D., 2017. Regularization for deep learning: A taxonomy. URL: <https://arxiv.org/abs/1710.10686>, arXiv:1710.10686.
- Lee, K., Carlberg, K., 2019. Model reduction of dynamical systems on nonlinear manifolds using deep convolutional autoencoders. URL: <https://arxiv.org/abs/1812.08373>, arXiv:1812.08373.
- Michelucci, U., 2022. An introduction to autoencoders. URL: <https://arxiv.org/abs/2201.03898>, arXiv:2201.03898.
- Rumelhart, D.E., Hinton, G.E., Williams, R.J., 1986. Learning internal representations by error propagation, in: Rumelhart, D.E., McClelland, J.L. (Eds.), *Parallel Distributed Processing: Explorations in the Microstructure of Cognition, Volume 1: Foundations*. MIT Press, Cambridge, MA, pp. 318–362.
- Sirignano, J., 2016. Deep learning for limit order books. URL: <https://arxiv.org/abs/1601.01987>, arXiv:1601.01987.
- Smith, L.N., 2017. Cyclical learning rates for training neural networks. URL: <https://arxiv.org/abs/1506.01186>, arXiv:1506.01186.
- Way, G., Zietz, M., Rubinetti, V., Himmelstein, D., Greene, C., 2020. Compressing gene expression data using multiple latent space dimensionalities learns complementary biological representations. *Genome Biology* 21. doi:10.1186/s13059-020-02021-3.